Achieving excellent ductility in high-strength Mg-10.6Gd-2Ag alloy *via* equal channel angular pressing

Jiapeng Sun[1], Bingqian Xu[1], Zhenquan Yang[1], Hao Zhou[2], Jing Han[3], Yuna Wu[1], Dan Song[1], Yuchun Yuan[1], Xioru Zhuo[1], Huan Liu[1,*], Aibin Ma[1,*]

1. College of Mechanics and Materials, Hohai University, Nanjing 210098, China;
2. Nano and Heterogeneous Material Center, School of Materials Science and Engineering, Nanjing University of Science and Technology, Nanjing, 210094, China
3. School of Mechanical and Electrical Engineering, China University of Mining and Technology, Xuzhou 221116, China

* Correspondence: liuhuanseu@hhu.edu.cn (Huan Liu); aibin-ma@hhu.edu.cn (Aibin Ma)

Abstract: Excellent ductility and high strength were achieved in the Mg-10.6Gd-2Ag (wt. %) alloy *via* an industrial-scale equal channel angular pressing (ECAP). The ECAP alloy exhibits an extremely high ductility (elongation of 22.6 %) as well as a high strength (ultimate tensile strength of 417.2 MPa). This ductility exceeds the known ductility limit of the existing high-strength Mg-RE wrought alloys. After peak-aging, an optimal ultimate tensile strength of 460.3 MPa is obtained accompanied by a moderate ductility (elongation of 8.9 %). The excellent ductility originates from the fine and full DRXed microstructure, which involves the homogenous and fine equiaxed grains, the cobblestone-like submicron particles distributed along the α-Mg grain boundaries, and the weak and approximately random texture. The submicron particles are identified as the dynamically precipitated Ag-containing Mg_5Gd-typed compound. After peak-aging, co-existence of the high-density basal γ'' plates and the relatively low-density prismatic β' plates are observed in the α-Mg grain interior, and an interfacial phase is found to segregate in some α-Mg grain boundaries. The high strength is mainly ascribed to the synergistic effect of the fine grains, the high-frequency high angle boundaries, and the additional co-precipitates of the β' plates and the γ'' plates in the aged alloy.

Keywords: Mg-Gd-Ag alloy; Mechanical property; ECAP; Microstructure; Precipitate.

1. Introduction

Mg alloys are the lightest structural metallic materials and thus possess many advantages such as high specific strength and high specific stiffness, which exhibits very attractive application potential, especially in the automobile, aircraft and 3C

industries. However, the absolute strength and ductility of the current developed Mg alloys at room temperature are still much lower than that of Al alloys and steels, which restrict their widespread commercial applications. Developing high strength and ductility Mg alloys is still a great challenge.

If we define that the high-strength Mg alloys are those with ultimate tensile strength (UTS) of above 400 MPa, it can be found that almost all the high-strength Mg alloys are the alloys containing rare earth elements (Mg-RE alloys) and achieve high strength *via* heat deformation process combined with heat treatment. The analysis of the published literature shows that the majority of the developed high-strength Mg-Re alloys so far have a poor ductility (elongation < 10 %) [1, 2], and thus the strength-ductility trade-off is extremely outstanding in these alloys. For example, Le *et al*. [3] reported the Mg-6Gd-3Y-2Nd-0.4Zr (wt%) alloy prepared by the combined processes of hot extrusion and aging exhibited a high UTS of 435 MPa companied by a low elongation (EL) of 5%. Recently, Yu *et al*. [4] developed a high-strength Mg-11.7Gd-4.9Y-0.3Zr (wt%) alloy with UTS of 500 MPa via the route of pre-deformation annealing, hot extrusion, and aging process, while a low ductility (elongation of 2.7%) is still inevitable. In these alloys, high strength is generally ascribed to the fine gains, strong basal texture and high-density nano-precipitates, such as β', β'', γ' and γ'' phases [5, 6]. To further improve the mechanical properties, a high RE concentration (>13%) and complicated processing route are necessary [7-9], which increases the cost and density of the alloys and thus weakens their lightweight advantage.

Recent researches demonstrated that the addition of silver (Ag) could enhance the hardness and strength of the Mg-Gd alloys *via* forming the nano-scale plate-like precipitates on basal plane during aging [10-13]. Although a high strength, even over 600 MPa, can be obtained in Ag-containing Mg-Gd alloys, a poor ductility is still outstanding [14-16]. This is because the inter-precipitate spacing is usually only a few nanometers, which significantly hinders dislocation slip and twinning. In this work, we conducted an industrial-scale ECAP on the developed Mg-10.6Gd-2Ag (wt. %) alloy followed by post-aging to obtain high strength and ductility. The excellent ductility (elongation of 22.6 %) and high strength (> 400 MPa) were achieved in the ECAP alloy, which jumps out of the ‘banana curve’ region of the high-strength Mg-RE wrought alloys containing comparable alloying addition (< 13 wt. %). The microstructures of this alloy at different processing states were characterized and carefully linked to its mechanical properties to reveal the underlying strengthening and toughening mechanism.

2. Materials and Methods

Ternary Mg-10.6Gd-2Ag alloy (wt. %) ingots with a diameter of 900 mm were prepared using the die-casting process. The ingot was machined into the cubic samples with dimensions of 50 mm × 50 mm × 100 mm for the subsequent process. The cubic samples were firstly solid solution treated at 773 K for 24 h followed by the water quenching, and the resultant alloy was designated as 'ss alloy'. Then, a rotational die equal channel angular pressing (ECAP) with two equal square channels (50 mm × 50 mm × 100 mm) was continually conducted on the samples for 8 passes with a ram speed of 3 mm/s at a constant temperature of 623 K, followed by the water cooling. The resultant alloy was signed as 'ECAP alloy'. Finally, some ECAP samples were isothermally aged at 453 K. The peak-aged ECAP alloy was named as 'ECAP-aged alloy'. The sample was lubricated by the grease mixed with molybdenum disulfide and graphite to reduce the friction. The detailed operation principle of the RD-ECAP can be found in our earlier work [17, 18]. Due to the friction between die and samples, the circumference of the samples shows different deformation and resultant microstructure and properties from their middle during ECAP. Hence, the outermost layer (5 mm in thickness) of the ECAP and ECAP-aged alloys was excised, and the middle layer was used to investigate the microstructure and mechanical behavior. Previous reports indicated that the whole microstructure became much homogenized after multi-passes ECAP [18]. Therefore, the samples for microstructure characterization and mechanical properties testing were randomly chosen from the middle of the ECAP and ECAP-aged alloys. The observed consistency of the microstructure observations and the small deviation of mechanical properties confirm the uniformity of the ECAP and ECAP-aged alloys (much more on this later).

The microstructures were characterized by an optical microscope (OM) Olympus BX51M, an electron backscattered diffraction (EBSD) HKL-EBSD system and a transmission electron microscope (TEM) FEI Tecnai G2. The OM samples were prepared by grinding, polishing and etching. The EBSD samples were ground and polished, and then ion polished. The TEM samples were prepared via twin-jet polishing with a solution of 2% perchloric ethanol at 253 K. The phase composition was measured by X-ray diffraction (XRD).

Tensile tests were conducted using a testing machine SUNS UTM4204X at room temperature with a constant tensile speed of 0.5 mm/min. The dog-bone shaped specimens with a gauge size of 2 mm × 2 mm × 7.5 mm were used. At least three

measurements were performed for each condition. The micro-hardness was measured using an HXD-1000TC microhardness-testing instrument on the surface of the sample. The applied load was 4.9 N, and the holding duration was 15 s. The average microhardness value of the eight test points was used.

3. Results and discussion

3.1 The age-hardening response of the ECAP alloy

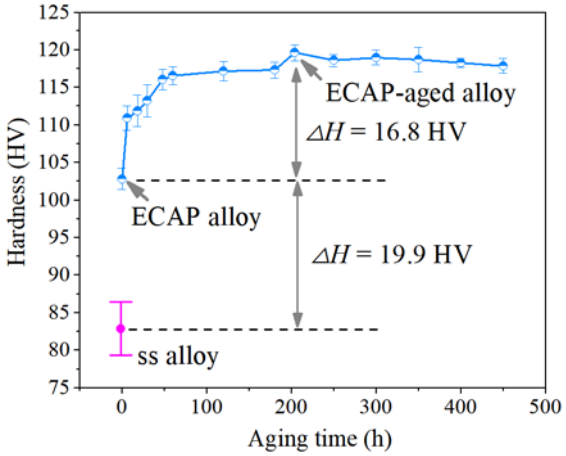

Fig. 1 Hardness curves of the ECAP alloy at 453 K.

Fig. 1 shows the age-hardening curve of the ECAP alloy during isothermal aging at 453 K. On the start of the aging, the hardness increases immediately without any incubation time until 60 hours, and then slowly increases to its peak value of 119.6 HV at 204 hours. After that, the hardness slowly declines with the increase in the aging time. The accelerated hardening at an early stage could be linked to the addition of Ag [11]. The hardness increase (ΔH) of the ECAP-aged alloy (i.e., the peak-aged alloy) is 16.8 HV compared to the ECAP alloy. Interestingly, the hardness increase of the ECAP alloy is 19.9 HV compared to ss alloy. This indicates that the aging treatment gives rise to comparable improvement in hardness to the ECAP processing for the Mg-10.6Gd-2Ag alloy.

3.2 Microstructure evolution during processing

Fig. 2a shows the optical microstructure of the Mg-10.6Gd-2Ag alloy in different processing states. A dendritic structure with a typical grain size of about 150 μm characterizes the microstructure of the as-cast alloy. This dendritic structure consists of the primary α-Mg and interdendritic eutectic in which the second phase is dispersed along the grain boundaries of the primary α-Mg. After solid solution treatment at 773 K for 24 h, most of the eutectic structure is disappeared, while some discontinuous

second phase particles are still visible in the α-Mg matrix, as shown in Fig. 2b. The average grain size of the ss alloy reaches to 187.5 ± 24.4 μm, indicating visible grain growth during solid solution treating. After 8 passes ECAP, the grain size is significantly decreased, as shown in Fig. 2c. Also, plenty of particles are uniformly dispersed in the refined α-Mg matrix, indicating that the ECAP processing involves intensive dynamical precipitation. As a result, a uniform microstructure is achieved in the ECAP alloy. After further aging to peak hardness, negligible change is found in optical microstructure, implying nano-precipitates are formed in the ECAP-aged alloy considering its improved hardness.

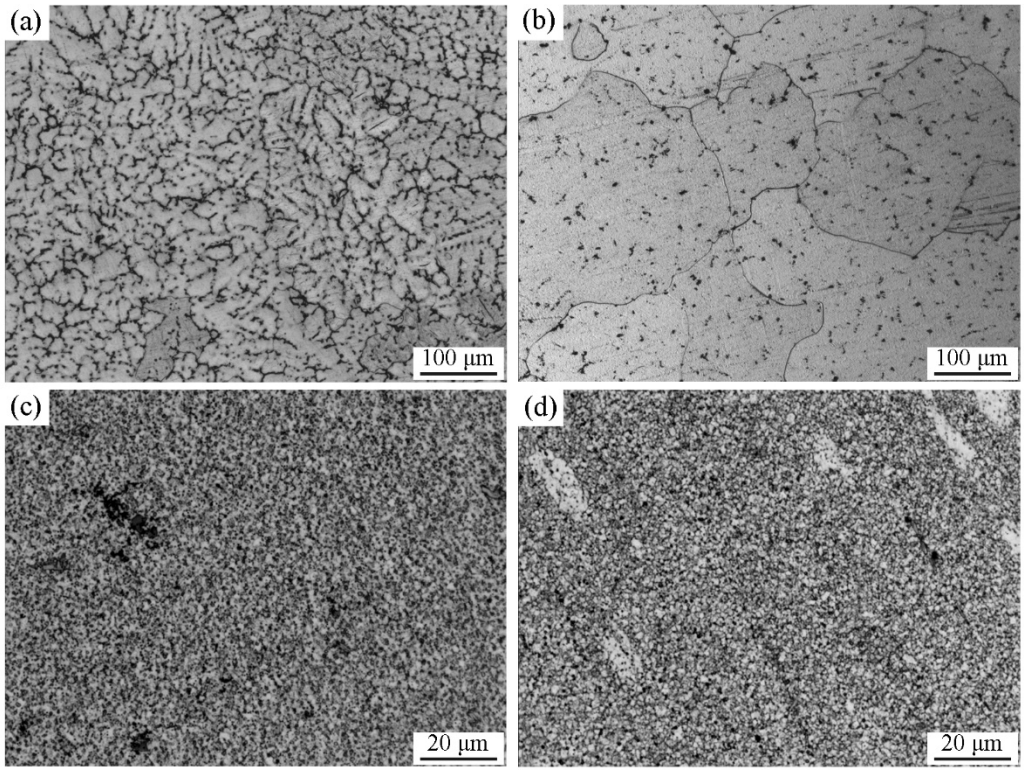

Fig. 2 Optical microstructure of (a) the as-cast alloy, (b) the ss alloy, (c) the ECAP alloy and (d) the ECAP-aged alloy.

Fig. 3 shows the XRD patterns of the Mg-10.6Gd-2Ag alloy in different processing states to reveal the phase composition evolution. The characteristic peaks confirm that the as-cast alloy is composed of α-Mg and well-known Mg_5Gd phase which is widely observed in the as-cast Mg-Gd system alloys [19]. After solid solution treatment, the peaks representing the Mg_5Gd phase are almost disappeared, giving rise to an almost single-phase α-Mg solid solution. After 8 passes ECAP, the peaks representing the Mg_5Gd phase reappear but their intensities are weak compared to the as-cast alloy. This demonstrates that the precipitates during the ECAP processing are the Mg_5Gd phase

particles. After further aging to peak hardness, the XRD pattern has no remarkable change. Therefore, TEM observations are necessary to reveal the microstructure different between the ECAP alloy and the ECAP-aged alloy.

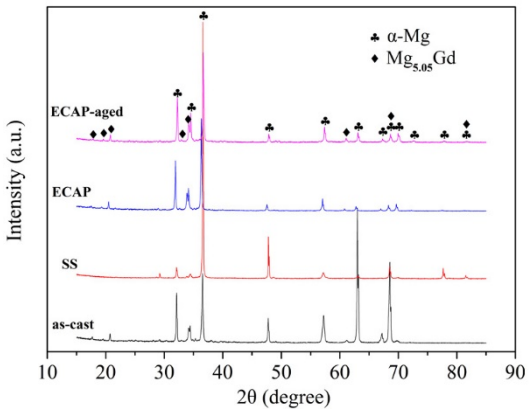

Fig. 3 XRD patterns of the as-cast alloy, the ss alloy, the ECAP alloy and the ECAP-aged alloy.

Fig. 4 shows the EBSD inverse pole figure mapping, grain size statistics, and pole figures of the ECAP alloy and the ECAP-aged alloy along extruding direction. Both the alloys possess the homogenous and fine equiaxed grains, as shown in Fig. 4a and d. The average grain size of the two alloys is comparable and less than 2 μm, which is much smaller than that of the as-cast alloy and the ss alloy. Both the alloys exhibit weak and approximately random texture, which is ascribed to the addition of rare earth elements, as shown in Fig. 4 c and f. Moreover, rare low-angle boundaries (LABs) are observed in the two alloys, which implies low dislocation density, as indicated in Fig. 4a and d. The equiaxed grains and rare LABs suggest that dynamical recrystallization (DRX) is well developed during the ECAP processing for the Mg-10.6Gd-2Ag alloy. As a result, the ECAP and ECAP-aged alloys exhibit stable and almost full DRXed grain microstructure, which implies excellent mechanical properties.

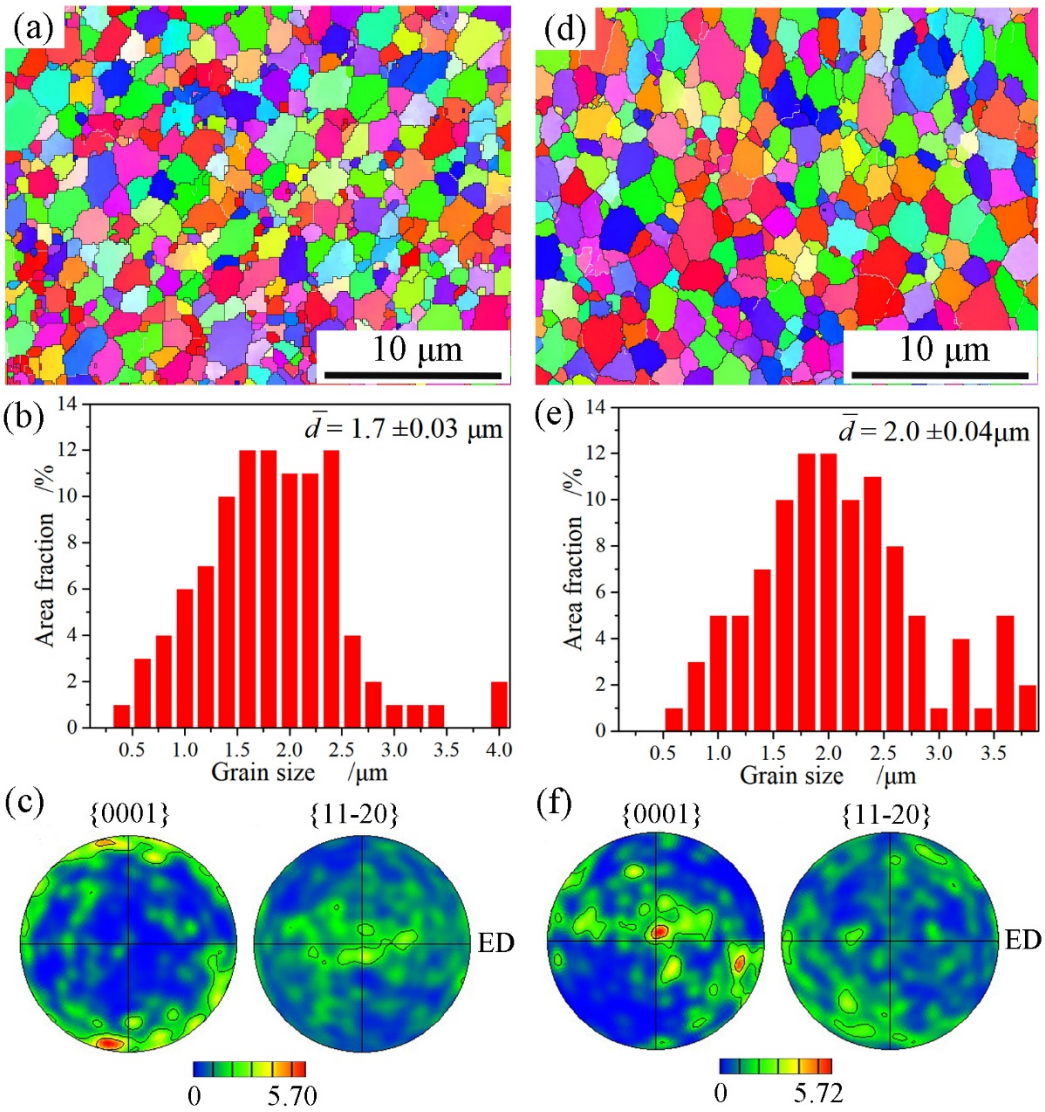

Fig. 4 (a, d) EBSD inverse pole figure mapping, (b, d) grain size statistics, and (c, f) pole figures of (a-c) the ECAP alloy and (d-f) the ECAP-aged alloy. The white curves in (a, d) mark the LABs ($2° < \theta < 15°$) and the black curves mark the high-angle boundaries (HABs, $\theta > 15°$).

Fig. 5 shows the bright-field (BF) images of the ECAP alloy before and after aging treatment. As shown in Fig. 5a, the fine equiaxed grains with low dislocation density are observed in the ECAP alloy. It indicates that a full DRX occurred during the ECAP processing. This result coincides with the EBSD result in Fig. 4. Moreover, plenty of the cobblestone-like precipitates, which have an average size of ~0.4 μm, are uniformly distributed along the α-Mg grain boundaries. Owing to their efficient inhibition in grain growth [20], these dynamically precipitated particles play an important role in the grain refinement during the ECAP processing. Previous studies hypothesized that this phase was the Ag-containing Mg_5Gd-typed compound [16, 21]. Our XRD analysis confirms

its Mg_5Gd-typed compound, while the exact composition of the dynamic precipitation is still unclear, which is worthy to be further studied in the future.

Compared with the two samples before and after aging (Fig. 5a and b), it is hard to tell the difference between the size of the grain boundary precipitates. However, a large number of the nano-precipitates are found in the α-Mg grain interior of the ECAP-aged alloy. To further clarify this precipitate microstructure of the ECAP-aged alloy, a high-magnification TEM BF image and corresponding selected area electron diffraction (SAED) pattern are given in Fig. 5c. The ECAP-aged alloy contains a large number of the uniformly distributed plate-like precipitates in basal planes as marked by yellow arrows in Fig. 5c, which exhibit a typical size of ~20 nm in length and ~1.5 nm in thickness. These precipitates were frequently observed in the aging treated Mg-Gd-Ag alloys, which were defined as γ'' phases [12, 13, 22]. Zhou *et al*. [23] indicated that the microstructure of the γ'' phase in the Mg-Gd-Y-Ag alloy was HCP, which had lattice parameters of a = 0.5 nm and c = 0.42 nm. The orientation of crystal structure was rotated for 30 degrees along c-axis of the matrix. The composition of γ" phase was proposed as $Mg_2Gd_1Ag_3$. Moreover, β' phase on a prismatic plane is also found to coexist with γ'' phase as marked by red arrows in Fig. 5c. The density of the β' phase is slightly lower than the γ'' phase. However, the β' phase is believed as the predominant precipitate phase in peak-aged Mg-Gd(-Zr) alloys, which has a base-centered orthorhombic Bravais lattice (a = 0.650 nm, b = 2.272 nm, and c = 0.521 nm) [22]. The dark diffraction spots and streaks, as marked by green arrows in the inset of Fig. 5c, further confirm the co-existence of the γ'' plates and the prismatic β' plates in the ECAP-aged alloys [22, 24]. The β' phase operates in conjunction with the γ'' phase to obstructed both the basal slip and non-basal slip in Mg, which is effective to enhance the mechanical properties of the Mg alloys [10, 22, 25, 26].

Some grain boundaries of the ECAP-aged alloy are segregated by an interfacial phase, as marked by blue arrows in Fig. 5b. High-magnification TEM BF image indicates that the interfacial phase is similar to the conventional precipitates segregated at grain boundaries (Fig. 5d). Zhou *et al*. [10] demonstrated that this interfacial phase was a monoclinic structure with a stoichiometry of Mg_4GdAg_3, which had lattice parameters of a = 1.2 nm, b = 1.04 nm, and c = 1.59 nm. Ag segregation to grain boundaries played a critical role in the formation of this interfacial phase. The grain boundaries with interfacial phase are regarded to be high stability due to the low energy nature, which exhibits huge potential in tuning the microstructure and mechanical properties [27-30].

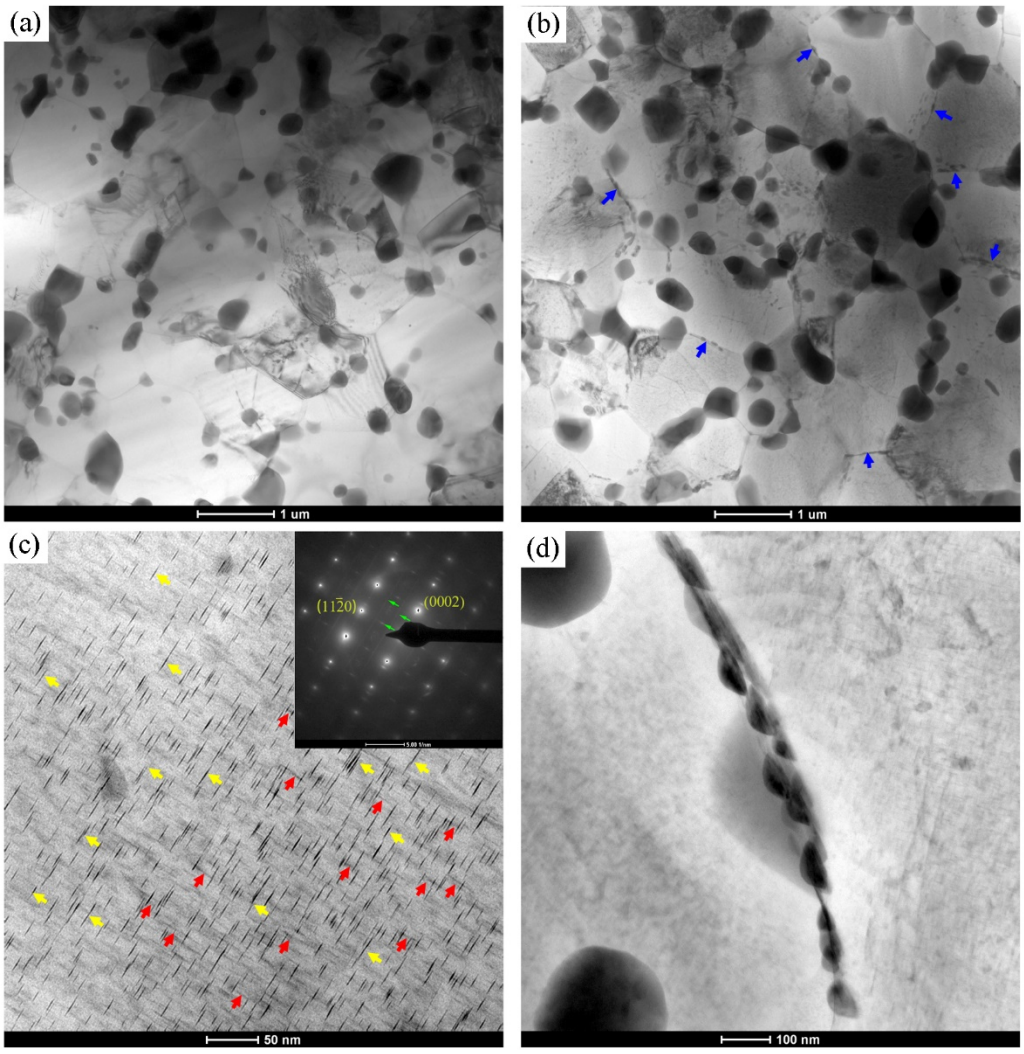

Fig. 5 TEM BF images of (a) the ECAP alloy and (b-d) ECAP-aged alloys. Enlargement of (c) a typical grain and (d) a grain boundary segregated by interfacial phase in ECAP-aged alloy. The inset in (c) shows the corresponding $[10\bar{1}0]_{\alpha}$ SAED pattern.

3.3 Mechanical properties

Fig. 6a and b show the typical tensile stress-strain curves and collected mechanical properties of the as-cast, ECAP, and ECAP-aged alloys. The ECAP alloy exhibits a high tensile yield strength (TYS) of 317.1 MPa and a ultimate tensile strength (UTS) of 417.2 MPa, as well as an extremely high elongation (EL) of 22.6 %, which are three times as strong (UTS) and two times as ductility as the as-cast alloy. This states a simultaneously improved strength and ductility compared to the as-cast alloy. After peak-aging, an optimal strength (TYS of 396.4 MPa and UTS of 460.3 MPa) is obtained accompanied by a moderate ductility (EL of 8.9 %).

The UTS of the typical high-strength Mg-RE wrought alloys with alloying addition < 13 wt. % are compared, including the present Mg-10.6Gd-2Ag alloy and the reported Zn-free Mg-RE alloys [3], Mg-Y-Zn alloys [31-34], Mg-Zn-RE alloys [35, 36], as shown in Fig. 6c. The high-strength Mg-RE wrought alloys generally undergo a trade-off between the strength and ductility, especially suffer a disadvantage of poor ductility. The comparison shows that the present ECAP alloy and the ECAP-aged alloy jump out of the 'banana curve' region, and can exceed the known strength and ductility limits of the high-strength Mg-RE wrought alloys containing comparable alloying addition. To our knowledge, the ductility of the present ECAP alloy exceeds that of all the reported high-strength Mg-RE wrought alloys (UTS > 400 MPa) [1, 2]. Although some Mg-RE wrought alloys possess higher strength than the present alloy, the higher alloying addition is necessary [1]. The results clearly show that the Mg-10.6Gd-2Ag alloy is in a region of high strength, good ductility and low alloying.

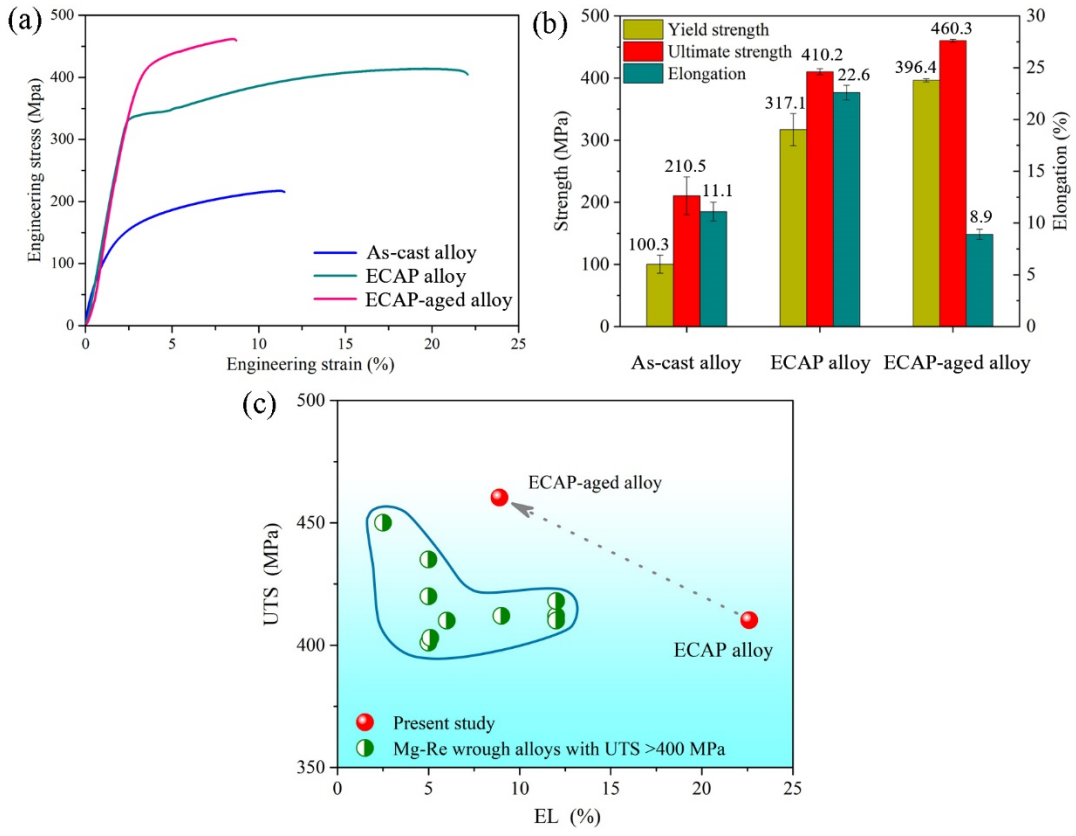

Fig. 6 (a) Typical tensile stress-strain curves and (b) mechanical properties of the as-cast, ECAP and ECAP-aged alloys. (c) Comparison of UTS *vs*. EL for the present Mg-10.6Gd-2Ag alloy and recently developed high-strength Mg-RE alloys [3, 30-35].

The high strength and excellent ductility in the present ECAP and ECAP-aged alloys can be linked to those microstructures. The alloys feature the complex structures

of (i) the fine and full DRXed α-Mg grains with the average size less than 2 μm, (ii) the high-frequency HABs, (iii) the homogeneously distributed submicron precipitates, (iv) the additional high-density nano-precipitates in the ECAP-aged alloy. The high strength originates from the compound effect of the above microstructures. Firstly, the fine grains are responsible for the enhanced strength by restricting dislocation slipping, as expressed by well-known Hall-Petch (HP) relationship ($\sigma_y = \sigma_0 + k_{HP}d^{-0.5}$), where d is the average grain size, σ_0 is the friction stress and k_{HP} is the HP constant. The fine grains can also reduce stress concentration and preventing necking, and may activate other deformation modes, such as grain boundary sliding, grain boundary rotation in Mg alloy, and thus contribute to enhanced ductility [37]. Moreover, the full DRXed α-Mg grains with low-density dislocations can accumulate abundant dislocations in grain interior. The dislocation storage provides work hardening and suppresses strain instability with macroscopic necking, and thus increases the ductility. Secondly, HABs with misorientation over 15 ° is widely believed to possess higher resistance to dislocation slipping than LABs. Herein, the high-frequency HABs contribute to a great improvement in strength. Their contribution can be coupled to the HP relationship, i.e., modified HP relationship [$\triangle\sigma_y = k_{HP}(d/f)^{-0.5}$], where f is the number fraction of HABs [38]. Alternatively, the average grain size is obtained just considering HABs, i.e., neglecting subgrains. From previous studies on AZ31, k_{HP} is in a range of 161 ~ 411 MPa·μm$^{0.5}$ [39], the calculated TYS increment due to the fine grains and HABs is in a range of 118.53 ~ 302.58 MPa. Thirdly, a large number of the submicron precipitates also contribute to improvement in strength *via* Orowan mechanism ($\sigma_{Orowan} = \frac{MGb}{2\pi\lambda\sqrt{1-\nu}} log\frac{d_p}{b}$), where M (=2.5) is the Taylor factor, G (=17.2 GPa) is the shear modulus of α-Mg matrix, b (= 0.32 nm) is the Burgers vector of the gliding dislocations, ν (= 0.3) is the Poisson ratio, λ is the effective inter-precipitate spacing, and is approximately equal to the average grain size, and d_p is the mean planar diameter of the precipitates on the slip planes [38]. The strength increment due to Orowan strengthening in the ECAP alloy and the ECAP-aged alloy are calculated to be 6.35 MPa and 5.47 MPa. Finally, the high-density nano-precipitates provide an additional strengthening effect in the ECAP-aged alloy. The co-existence of the β' phase and the γ'' phase precipitates is regard to effectively contribute to the strengthening of the Ag-containing Mg-Gd alloy by suppressing both the basal slip and non-basal slip [10, 22, 25, 26]. The resultant strength increment is equal to the strength difference between the ECAP-aged alloy and the ECAP alloy (79.3MPa). Therefore, the high strength mainly stems from the synergistic effect of the fine grain structure, the high-frequency HABs,

and the additional co-precipitates of the β' phase and the γ'' phase in the ECAP-aged alloy. The excellent ductility originates from the fine and full DRXed α-Mg grains.

4 Conclusion

In summary, we have developed a high-strength Mg-10.6Gd-2Ag alloy *via* an industrial-scale ECAP. Excellent ductility and high strength were achieved in this alloy. The main conclusions can be made as follows:

(1) The ECAP alloy exhibits an extremely high ductility (EL of 22.6 %) which exceeds the known ductility limit of the high-strength Mg-RE wrought alloys (UTS > 400 MPa), as well as a high strength (TYS of 317.1 MPa and UTS of 417.2 MPa). After peak-aging, an optimal strength (TYS of 396.4 MPa and UTS of 460.3 MPa) is obtained accompanied by a moderate ductility (EL of 8.9 %), which jumps out of the 'banana curve' region of the existing high-strength Mg-RE wrought alloys containing comparable alloying addition (< 13 wt. %).

(2) The ECAP alloy possesses a full DRXed microstructure, which involves the homogenous and fine equiaxed grains, the cobblestone-like submicron particles distributed along the α-Mg grain boundaries, and the weak and approximately random texture. The average grain size is less than 2 μm. These submicron particles are identified as the dynamically precipitated Ag-containing Mg_5Gd-typed compound during ECAP processing.

(3) At peak-aged condition, co-existence of the high-density basal γ'' plates and the relatively low-density prismatic β' plates are observed in the α-Mg grain interior, which is regard to effectively contribute to the strengthening of Mg alloy by suppressing both the basal slip and non-basal slip. An interfacial phase is also found to segregate in some grain boundaries, which endows these grains with high stability.

(4) The high strength mainly stems from the synergistic effect of the fine grain structure, the high-frequency HABs, and the additional co-precipitates of the β' plates and the γ'' plates in the ECAP-aged alloy. The excellent ductility originates from the fine and full DRXed α-Mg grains.

Acknowledgments

The authors acknowledge financial support received from the Natural Science Foundation of Jiangsu Province (Grant No. BK20160867 and BK20160869), the Fundamental Research Funds for the Central Universities (Grant No. 2017B12814 and

2018B48414), the National Natural Science Foundation of China (Grant No. 51605139, 51774109 and 51701065), the China Postdoctoral Science Foundation (2016M591752) and the Jiangsu Planned Projects for Postdoctoral Research Funds (Grant No. 1501041A).

References:

[1] J. Zhang, S. Liu, R. Wu, L. Hou, M. Zhang, Recent developments in high-strength Mg-RE-based alloys: Focusing on Mg-Gd and Mg-Y systems, J. Magnes. Alloy, 6(2018) 277-291.

[2] H. Liu, H. Huang, C. Wang, J. Sun, J. Bai, F. Xue, A. Ma, X. Chen, Recent Advances in LPSO-Containing Wrought Magnesium Alloys: Relationships Between Processing, Microstructure, and Mechanical Properties, Jom, (2019) online.

[3] X. Liu, W. Hu, Q. Le, Z. Zhang, L. Bao, J. Cui, Microstructures and mechanical properties of high performance Mg-6Gd-3Y-2Nd-0.4Zr alloy by indirect extrusion and aging treatment, Mat. Sci. Eng. A.-Struct., 612 (2014) 380-386.

[4] Z. Yu, C. Xu, J. Meng, S. Kamado, Microstructure evolution and mechanical properties of a high strength Mg-11.7Gd-4.9Y-0.3Zr (wt%) alloy prepared by pre-deformation annealing, hot extrusion and ageing, Mat. Sci. Eng. A.-Struct., 703 (2017) 348-358.

[5] J. Nie, Precipitation and Hardening in Magnesium Alloys, Metall. Mater. Trans. A., 43A (2012) 3891-3939.

[6] H. Zhou, W.Z. Xu, W.W. Jian, G.M. Cheng, X.L. Ma, W. Guo, S.N. Mathaudhu, Q.D. Wang, Y.T. Zhu, A new metastable precipitate phase in Mg-Gd-Y-Zr alloy, Philos. Mag., 94 (2014) 2403-2409.

[7] C. Xu, G.H. Fan, T. Nakata, X. Liang, Y.Q. Chi, X.G. Qiao, G.J. Cao, T.T. Zhang, M. Huang, K.S. Miao, M.Y. Zheng, S. Kamado, H.L. Xie, Deformation Behavior of Ultra-Strong and Ductile Mg-Gd-Y-Zn-Zr Alloy with Bimodal Microstructure, Metall. Mater. Trans. A., 49 (2018) 1931-1947.

[8] K. Yan, J. Sun, H. Liu, H. Cheng, J. Bai, X. Huang, Exceptional mechanical properties of an Mg97Y2Zn1 alloy wire strengthened by dispersive LPSO particle clusters, Mater. Lett., 242 (2019) 87-90.

[9] X. Zheng, W. Du, Z. Wang, S. Li, K. Liu, X. Du, Remarkably enhanced mechanical properties of Mg-8Gd-1Er-0.5Zr alloy on the route of extrusion, rolling and aging, Mater. Lett., 212 (2018) 155-158.

[10] L.R. Xiao, Y. Cao, S. Li, H. Zhou, X.L. Ma, L. Mao, X.C. Sha, Q.D. Wang, Y.T. Zhu, X.D. Han, The formation mechanism of a novel interfacial phase with high thermal stability in a Mg-Gd-Y-Ag-Zr alloy, Acta Mater., 162 (2019) 214-225.

[11] Y. Zhang, T. Alam, B. Gwalani, W. Rong, R. Banerjee, L. Peng, J. Nie, N. Birbilis, On the role of Ag in enhanced age hardening kinetics of Mg-Gd-Ag-Zr alloys, Phil. Mag. Lett., 96 (2016) 212-219.

[12] K. Yamada, H. Hoshikawa, S. Maki, T. Ozaki, Y. Kuroki, S. Kamado, Y. Kojima, Enhanced age-hardening and formation of plate precipitates in Mg-Gd-Ag alloys, Scripta Mater., 61 (2009) 636-639.

[13] X. Gao, J.F. Nie, Enhanced precipitation-hardening in Mg-Gd alloys containing Ag and Zn, Scripta Mater., 58 (2008) 619-622.

[14] W.W. Jian, G.M. Cheng, W.Z. Xu, H. Yuan, M.H. Tsai, Q.D. Wang, C.C. Koch, Y.T. Zhu, S.N. Mathaudhu, Ultrastrong Mg Alloy via Nano-spaced Stacking Faults, Mater. Res. Lett., 1 (2013) 61-66.

[15] Y. Zhang, W. Rong, Y. Wu, L. Peng, J. Nie, N. Birbilis, A comparative study of the role of Ag in microstructures and mechanical properties of Mg-Gd and Mg-Y alloys, Mat. Sci. Eng. A.-Struct., 731 (2018) 609-622.

[16] B. Wang, C. Liu, Y. Gao, S. Jiang, Z. Chen, Z. Luo, Microstructure evolution and mechanical properties of Mg-Gd-Y-Ag-Zr alloy fabricated by multidirectional forging and ageing treatment, Mat. Sci. Eng. A.-Struct., 702 (2017) 22-28.
[17] J. Sun, Z. Yang, J. Han, T. Yuan, D. Song, Y. Wu, Y. Yuan, X. Zhuo, H. Liu, A. Ma, Enhanced quasi-isotropic ductility in bi-textured AZ91 Mg alloy processed by up-scaled RD-ECAP processing, J. Alloy. Compd., 780 (2019) 443-451.
[18] A. Ma, Y. Nishida, K. Suzuki, I. Shigematsu, N. Saito, Characteristics of plastic deformation by rotary-die equal-channel angular pressing, Scripta Mater., 52 (2005) 433-437.
[19] Y. Zhang, Y. Wu, L. Peng, P. Fu, F. Huang, W. Ding, Microstructure evolution and mechanical properties of an ultra-high strength casting Mg-5.6Gd-1.8Ag-0.4Zr alloy, J. Alloy. Compd., 615 (2014) 703-711.
[20] T. Homma, N. Kunito, S. Kamado, Fabrication of extraordinary high-strength magnesium alloy by hot extrusion, Scripta Mater., 61 (2009) 644-647.
[21] Q. Wang, J. Chen, Z. Zhao, S. He, Microstructure and super high strength of cast Mg-8.5Gd-2.3Y-1.8Ag-0.4Zr alloy, Mat. Sci. Eng. A.-Struct., 528 (2010) 323-328.
[22] Y. Zhang, Y. Zhu, W. Rong, Y. Wu, L. Peng, J. Nie, N. Birbilis, On the Precipitation in an Ag-Containing Mg-Gd-Zr Alloy, Metall. Mater. Trans. A., 49 (2018) 673-694.
[23] X. Sha, L. Xiao, X. Chen, G. Cheng, Y. Yu, D. Yin, H. Zhou, Atomic structure of γ″ phase in Mg-Gd-Y-Ag alloy induced by Ag addition, Philos. Mag., (2019) 1-13.
[24] J.F. Nie, K. Oh-ishi, X. Gao, K. Hono, Solute segregation and precipitation in a creep-resistant Mg–Gd–Zn alloy, Acta Mater., 56(2008) 6061-6076.
[25] H. Ning, Y. Yu, B. Gao, L. Xiao, L. Wen, Z. Yan, L. Li, X. Chen, Grain Refinement and Aging Hardening of the Mg-10Gd-3Y-2Ag-0.4Zr Alloy Produced by a Two-Step Forming Process, Materials, 11 (2018) 757.
[26] Y. Zhang, Y. Wu, L. Peng, P. Fu, F. Huang, W. Ding, Microstructure evolution and mechanical properties of an ultra-high strength casting Mg-15.6Gd-1.8Ag-0.4Zr alloy, J. Alloy. Compd., 615 (2014) 703-711.
[27] M. Bugnet, A. Kula, M. Niewczas, G.A. Botton, Segregation and clustering of solutes at grain boundaries in Mg-rare earth solid solutions, Acta Mater., 79 (2014) 66-73.
[28] M. Bugnet, A. Kula, M. Niewczas, G.A. Botton, Segregation and clustering of solutes at grain boundaries in Mg-rare earth solid solutions, Acta Mater., 79 (2014) 66-73.
[29] J.F. Nie, Y.M. Zhu, J.Z. Liu, X.Y. Fang, Periodic Segregation of Solute Atoms in Fully Coherent Twin Boundaries, Science, 340 (2013) 957-960.
[30] H. Zhou, G.M. Cheng, X.L. Ma, W.Z. Xu, S.N. Mathaudhu, Q.D. Wang, Y.T. Zhu, Effect of Ag on interfacial segregation in Mg-Gd-Y-(Ag)-Zr alloy, Acta Mater., 95 (2015) 20-29.
[31] J. Wang, P. Song, X. Zhou, X. Huang, F. Pan, Influence of the morphology of long-period stacking ordered phase on the mechanical properties of as-extruded Mg-5Zn-5Y-0.6Zr magnesium alloy, Mat. Sci. Eng. A.-Struct., 556 (2012) 68-75.
[32] B. Chen, D. Lin, X. Zeng, C. Lu, Microstructure and mechanical properties of ultrafine grained Mg97Y2Zn1 alloy processed by equal channel angular pressing, J. Alloy. Compd., 440 (2007) 94-100.
[33] Y. Kawamura, M. Yamasaki, Formation and Mechanical Properties of Mg97Zn1RE2 Alloys with Long-Period Stacking Ordered Structure, Mater. Trans., 48 (2007) 2986-2992.
[34] S. Yoshimoto, M. Yamasaki, Y. Kawamura, Microstructure and Mechanical Properties of Extruded Mg-Zn-Y Alloys with 14H Long Period Ordered Structure, Mater. Trans., 47 (2006) 959-965.

[35] H. Jiang, X. Qiao, C. Xu, S. Kamado, K. Wu, M. Zheng, Influence of size and distribution of W phase on strength and ductility of high strength Mg-5.1Zn-3.2Y-0.4Zr-0.4Ca alloy processed by indirect extrusion, J. Mater. Sci. Technol., 34 (2018) 277-283.
[36] L. Liu, X. Chen, F. Pan, S. Gao, C. Zhao, A new high-strength Mg-Zn-Ce-Y-Zr magnesium alloy, J. Alloy. Compd., 688 (2016) 537-541.
[37] R.Z. Valiev, T.G. Langdon, Principles of equal-channel angular pressing as a processing tool for grain refinement, Prog. Mater. Sci., 51 (2006) 881-981.
[38] H. Pan, G. Qin, Y. Huang, Y. Ren, X. Sha, X. Han, Z. Liu, C. Li, X. Wu, H. Chen, C. He, L. Chai, Y. Wang, J. Nie, Development of low-alloyed and rare-earth-free magnesium alloys having ultra-high strength, Acta Mater., 149 (2018) 350-363.
[39] H. Yu, Y. Xin, M. Wang, Q. Liu, Hall-Petch relationship in Mg alloys: A review, J. Mater. Sci. Technol., 34 (2018) 248-256.